

Journal of Materials Chemistry A

Supplementary Information

Selective control and characterization of the photoelectrochemical and electrocatalytic properties of copper oxide materials for efficient solar fuel production

Angel T. Garcia-Esparza,^{a,‡} Kevin Limkraisassiri,^{b,‡} Frederic Leroy,^c Shahid Rasul,^a Weili Yu,^a Liwei Lin^b and Kazuhiro Takanabe^{a*}

^a Division of Physical Sciences and Engineering, KAUST Catalysis Center (KCC), King Abdullah University of Science and Technology (KAUST), 4700 KAUST, Thuwal, 23955-6900 Saudi Arabia.

E-mail: kazuhiro.takanabe@kaust.edu.sa

^b Department of Mechanical Engineering, University of California, Berkeley, California 94720, USA.

^c Département Chimie Physique, Stockage et Conversion de l'énergie (SCE), École Nationale Supérieure de Chimie, de Biologie et de Physique (ENSCBP), Pessac 33607, France.

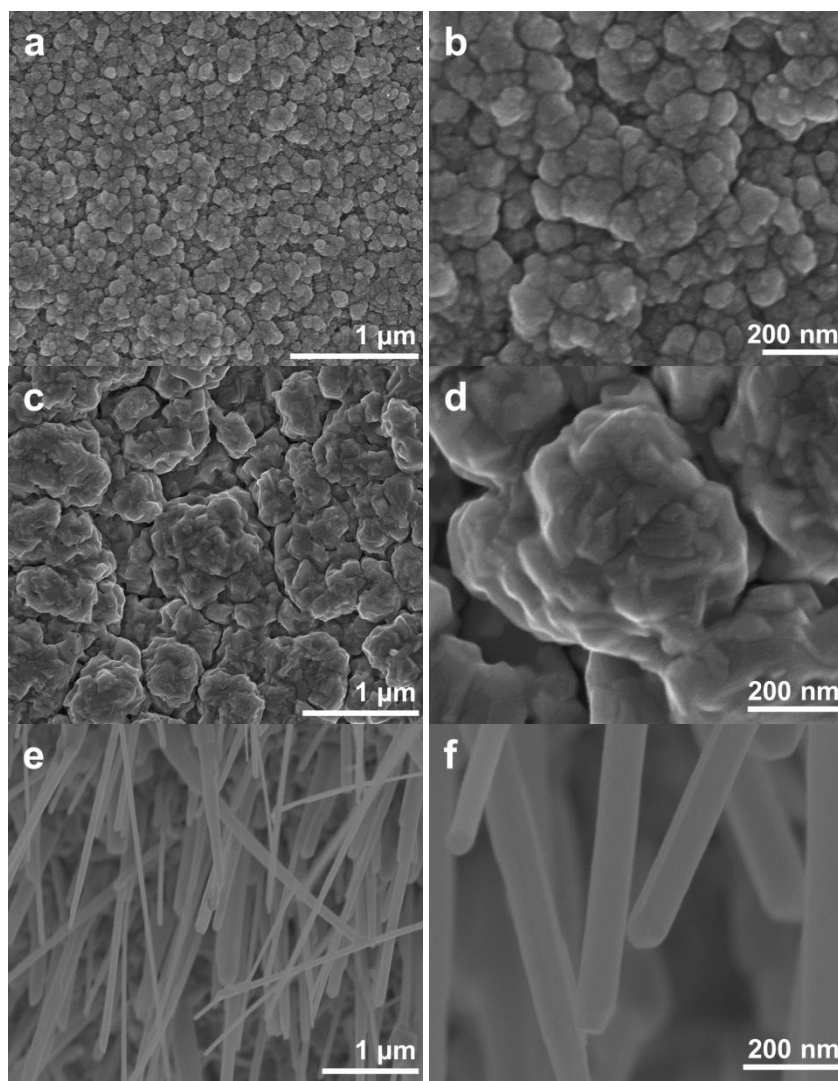


Fig. S1. SEM top view of the pristine (a, b) red, (c, d) deep red and (e, f) black samples.

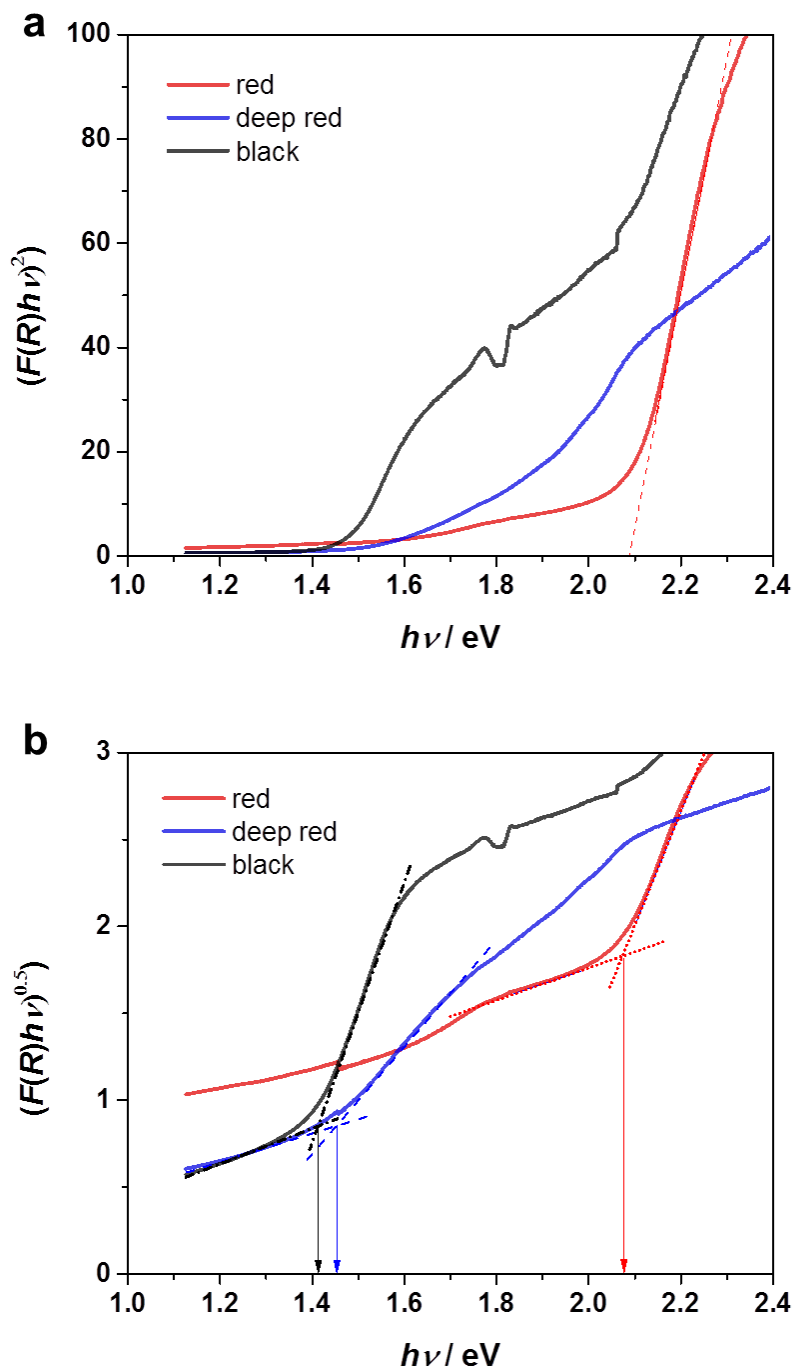


Fig. S2. (a) Allowed direct band gap and (b) allowed indirect band gap Tauc plots of the Cu-oxide-based materials obtained using the Kubelka-Munk radiative-transfer model assuming that $F(R)$ is proportional to the absorption coefficient.

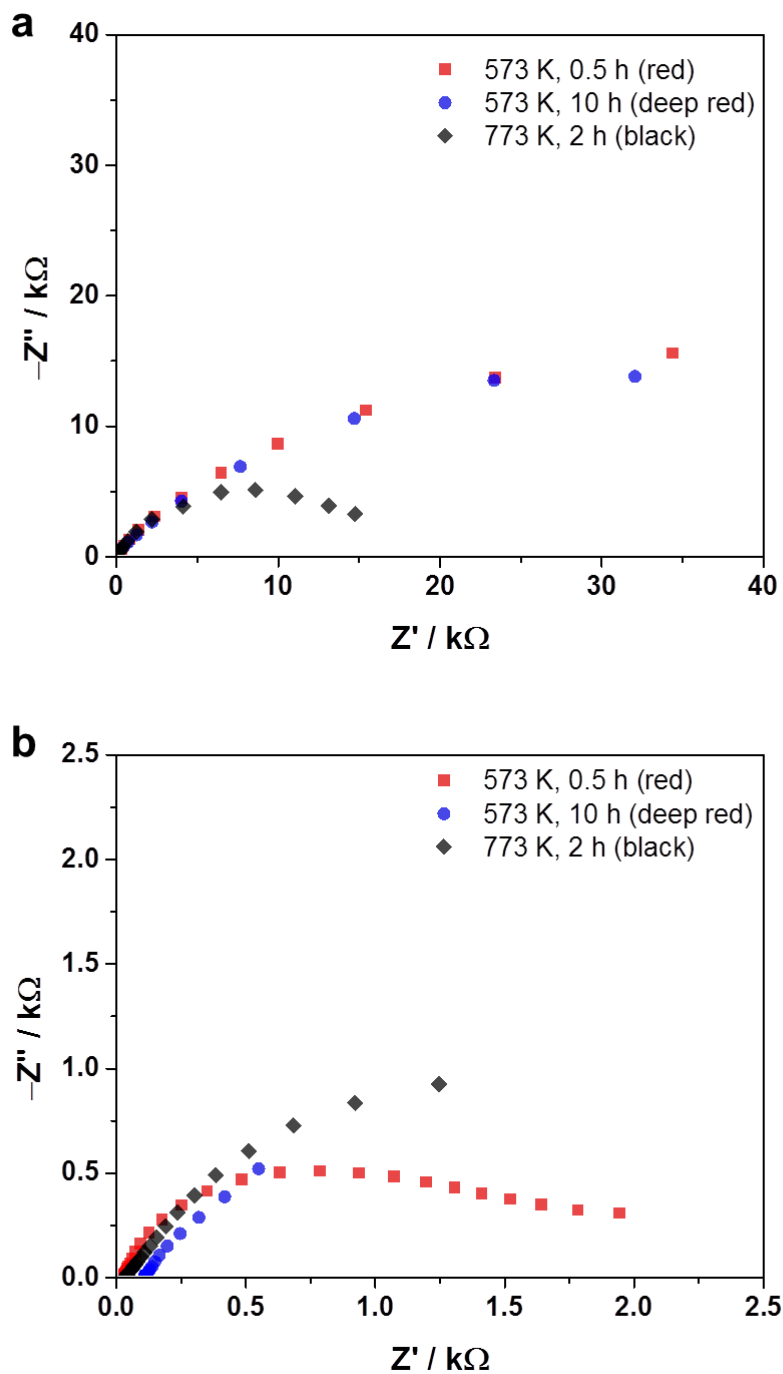


Fig. S3. Nyquist plots for the red, deep red and black samples at 0.55 V vs. RHE (a) before and (b) after the electrochemical-reduction step for the electrocatalysis of CO₂ reduction. The amplitude of the superimposed AC signal was 10 mV, and the probed frequency range was from 0.01 Hz to 100 kHz. (0.1 M sodium acetate, pH 7.9)

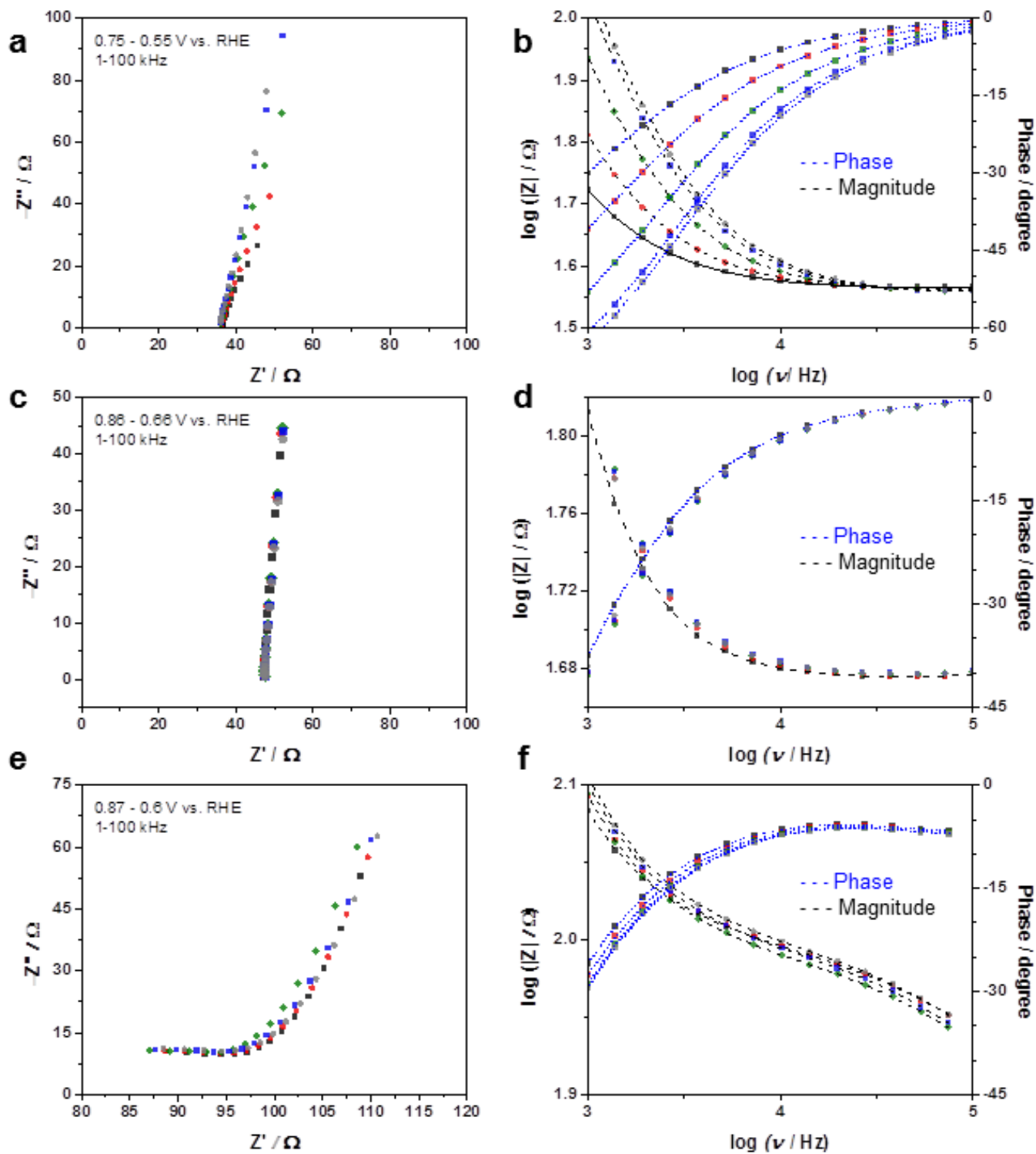


Fig. S4. Nyquist (left) and Bode (right) plots for the (a, b) red, (c, d) deep red and (e, f) black samples obtained from a “staircase”-potential electrochemical-impedance-spectroscopy measurement used to calculate the Mott-Schottky plots of the samples. The amplitude of the perturbation signal was 10 mV. (0.1 M sodium acetate, pH 7.9)

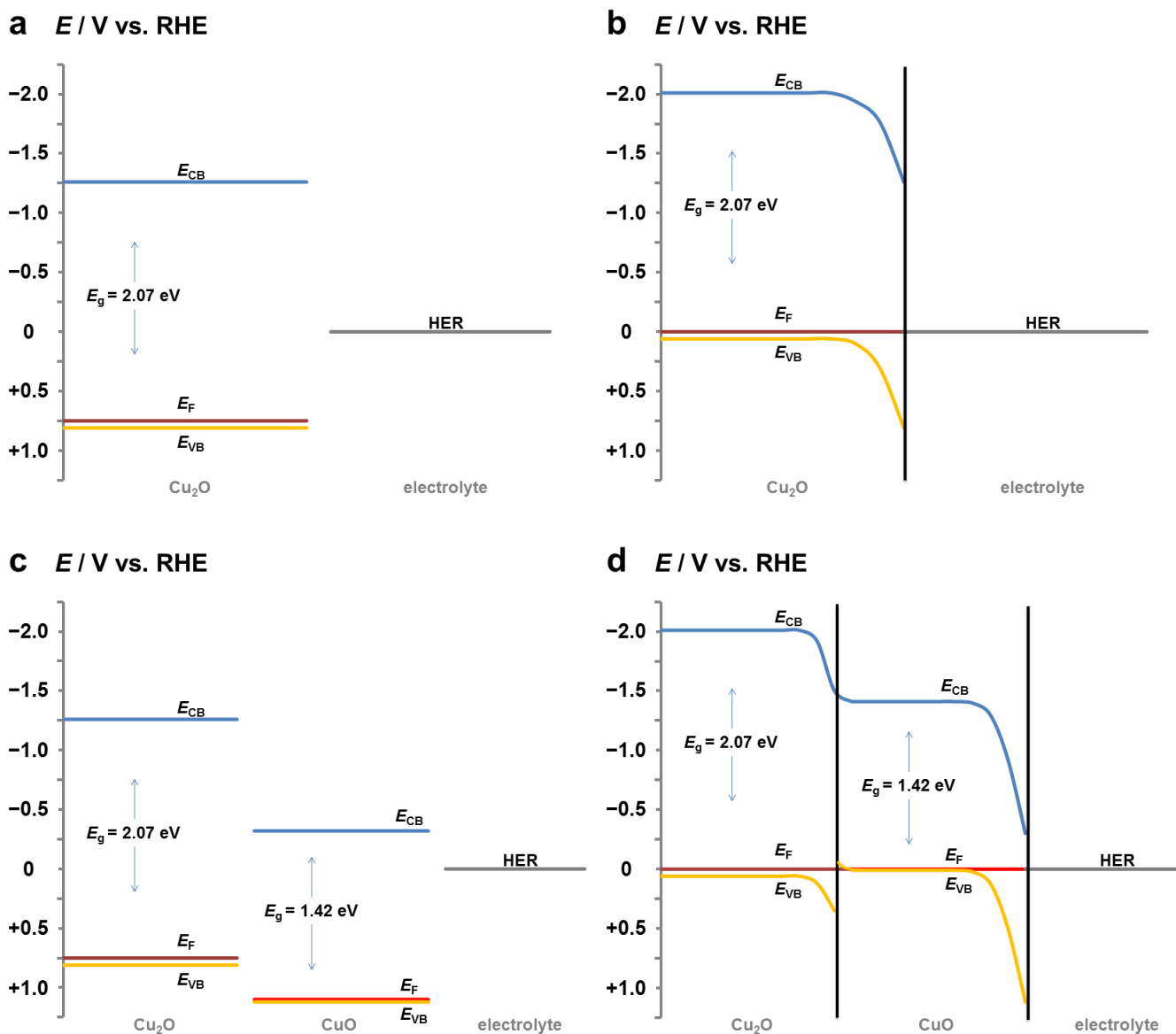


Fig. S5. Ideal representation of the energy-band diagrams for the (top a and b) red and (bottom c and d) black samples (a, c) before contact and (b, d) for the photocathodes biased at 0 V vs. RHE in the dark in contact with an electrolyte. A band-edge-pinning assumption was employed to schematically illustrate the band bending at the interface, taking the electrochemical potential of the solution to be the standard potential of the hydrogen evolution reaction (HER) and built-in potentials at the interfaces as the difference in Fermi levels.

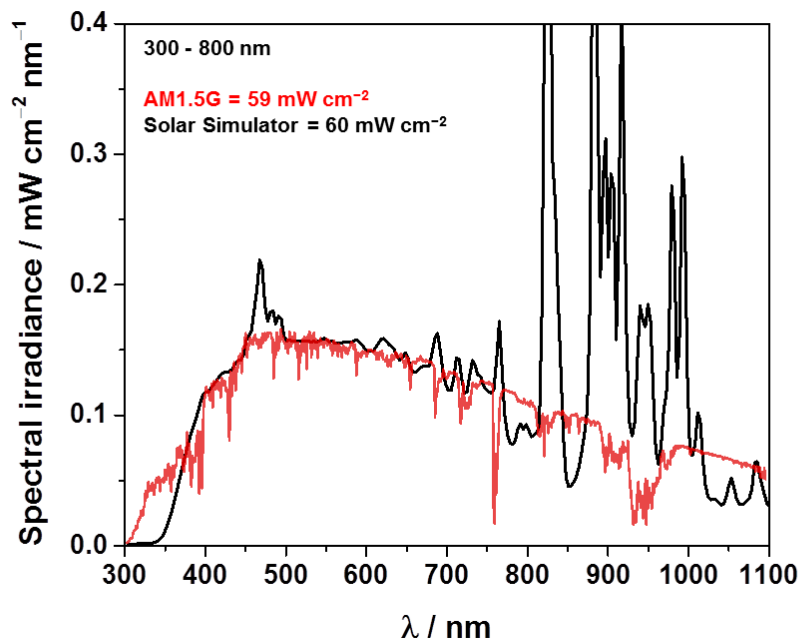


Fig. S6. Photon distribution of the solar simulator utilized for the photoelectrochemical characterization. The spectral irradiance (black line) was calibrated against the reference standard AM 1.5G (red line). The integrated spectral irradiance was calculated in the wavelength range of 300 to 800 nm.

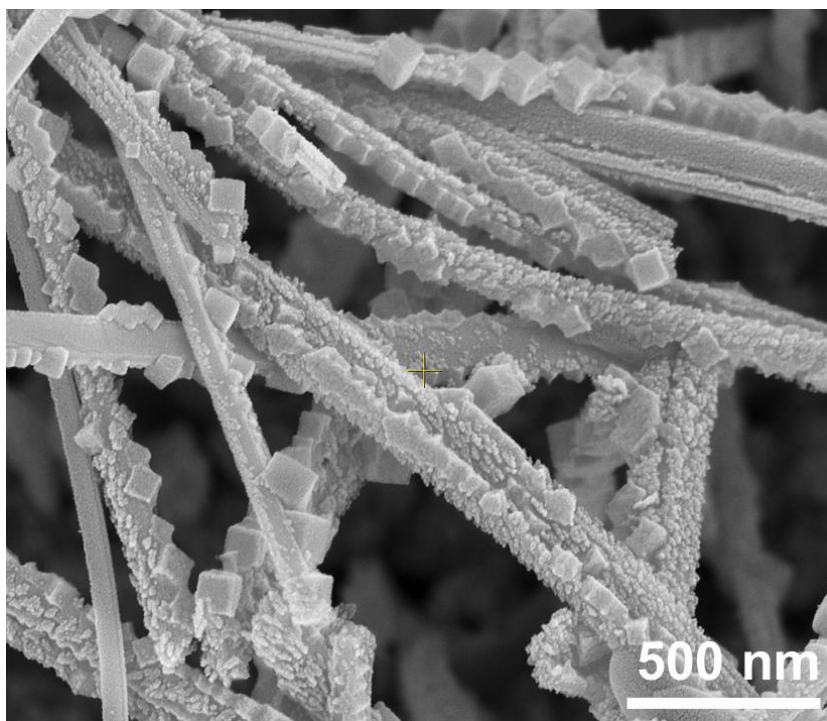


Fig. S7. Characteristic SEM micrograph of the black sample after a 20-minute photoelectrochemical stability test. The black sample was subjected to alternating 20 s periods of simulated solar illumination and dark conditions while a constant potential of 0.25 V vs. RHE was applied (AM 1.5G, 0.5 M Na₂SO₄, pH 6.1).

The observed cubic nanoparticle crystals on the surfaces of the nanowires may have originated from the reduction of Cu(II) to Cu(I) and metallic Cu, consistent with a previous report concerning electrodeposited Cu₂O.¹ The observation suggests that the photo-excited electrons generated in the Cu₂O can be collected by CuO and react at the electrolyte interface. This result establishes the possibility of electronic communication through the crystals (Cu₂O/CuO) and the plausible formation of a staggered *p-p* heterojunction.

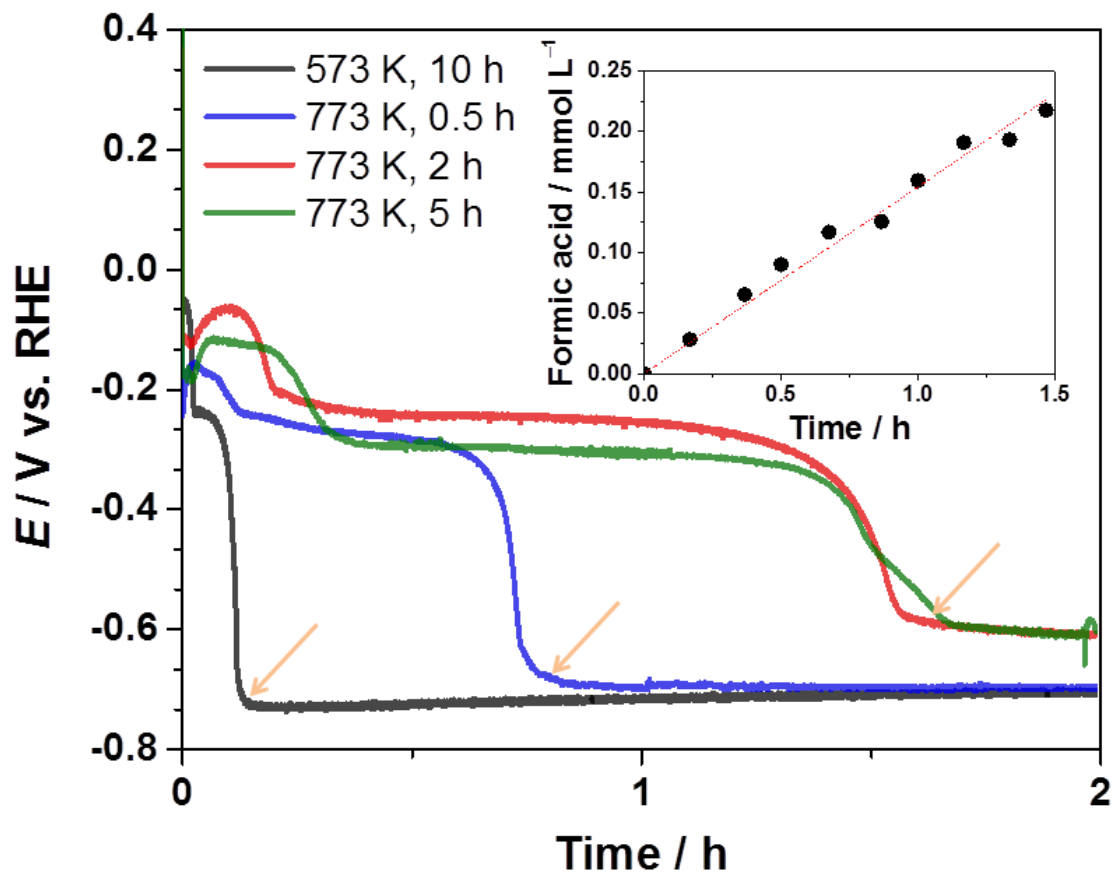


Fig. S8. Chronopotentiometry at a constant current of -5 mA was utilized to analyze samples treated at different temperatures and for different times. Liquid sampling was performed every 10 minutes using a septum, and the products were analyzed *via* HPLC. The arrows indicate the times when the potential was stabilized and the constant formation of gaseous (H_2 and/or CO) and liquid products were detected. Furthermore, it was also confirmed that no liquid products were formed (i.e., formic acid and/or acetic acid) prior to the potential stabilization (indicated by the arrows in the figure). The inset of the figure shows the steady-state production of formic acid for the black sample treated at 773 K for 2 h. (0.1 KHCO_3 , pH 6.8, saturated CO_2 , geometric area of 3 cm^2)

Table S1. Summary of Faradic efficiencies under potentiostatic control (-0.6 V vs. RHE) for all samples produced and their respective selectivities. Other hydrocarbons were not detected in this study. (0.1 M KHCO₃, pH 6.8, saturated CO₂, geometric area of 3 cm²)

	Annealing Time (h)	Faradaic efficiency (η)				Selectivity (%)			
		H ₂	CO	Formic acid	Acetic acid	H ₂	CO	Formic acid	Acetic acid
Cu	-	96	1	3	0	96	1	3	0
573 K	0.5	82	4	7	0	88	4	8	0
573 K	10	50	6	18	0	66	8	24	0
773 K	0.5	47	14	29	4	50	15	31	4
773 K	1	45	16	25	4	50	18	28	4
773 K	1.5	37	23	26	6	40	25	28	7
773 K	2	40	18	27	3	45	21	31	3
773 K	5	36	14	36	4	40	16	40	4
773 K	10	36	14	17	3	53	20	24	3

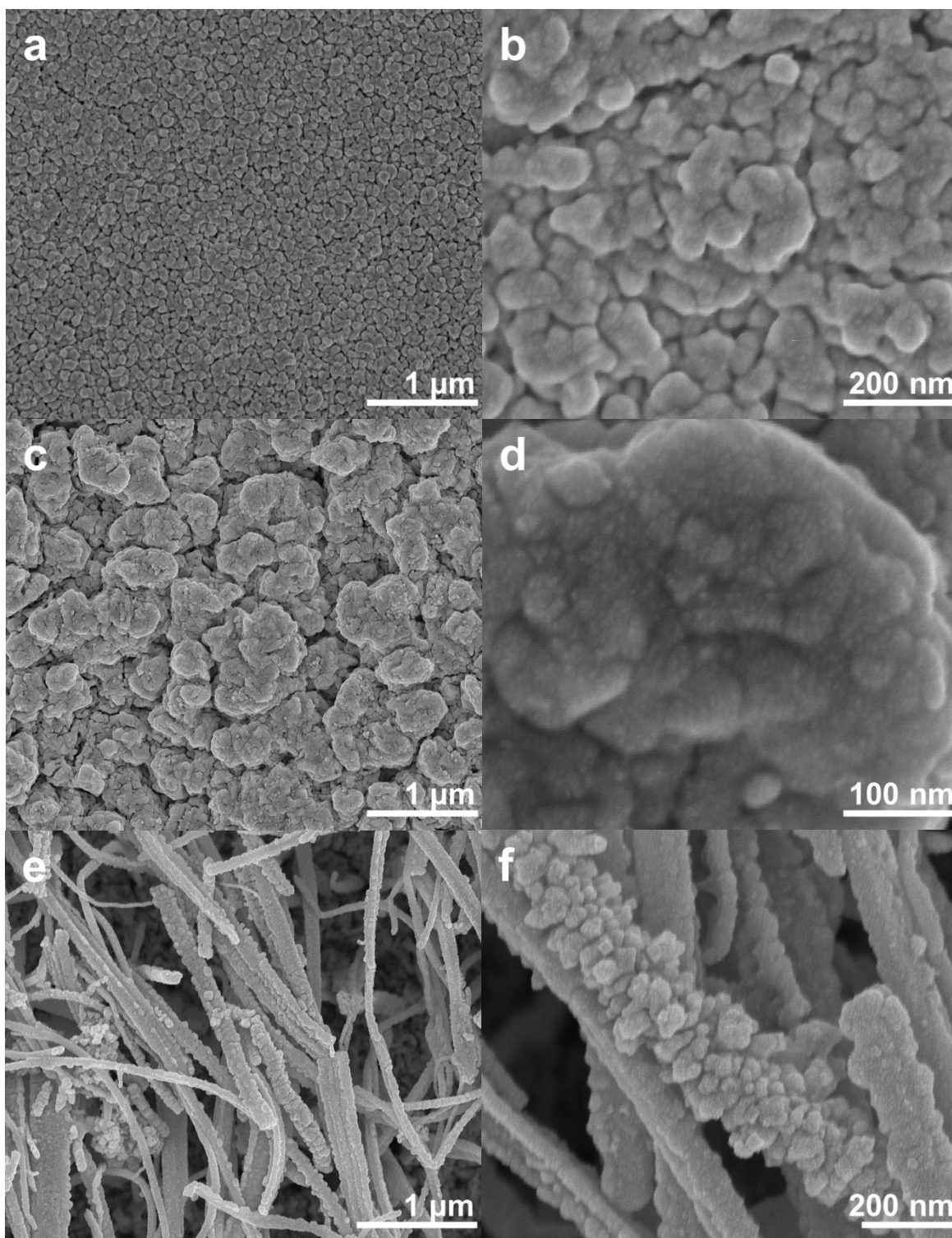


Fig. S9. SEM images of the (a) red, (b) deep red and (c) black samples after exposure to galvanostatic reduction conditions for 2 h during the electrochemical reduction of CO₂. Homogeneously distributed nanoparticles of various sizes (i.e., smaller than 10 nm) formed on the surfaces of the composites. (1.67 mA cm⁻², 0.1 M KHCO₃, CO₂ saturated, pH 6.8)

References (Supporting information)

1. A. Paracchino, V. Laporte, K. Sivula, M. Grätzel, and E. Thimsen, *Nat. Mater.*, 2011, **10**, 456–61.